JACS
JOURNAL OF THE AMERICAN CHEMICAL SOCIETY

ARTICLE

pubs.acs.org/JACS

Structure of the Oxygen-Rich Cluster Cation $Al_2O_7^+$ and its Reactivity toward Methane and Water

Zhe-Chen Wang,[†] Thomas Weiske,[†] Robert Kretschmer,[†] Maria Schlangen,*[,†] Martin Kaupp,[†] and Helmut Schwarz*[,†,‡]

[†]Institut für Chemie der Technischen Universität Berlin, Straße des 17. Juni 135, 10623 Berlin, Germany

[‡]Chemistry Department, Faculty of Science, King Abdulaziz University, Jeddah 21589, Saudi Arabia

Supporting Information

ABSTRACT: The oxygen-rich cluster $Al_2O_7^+$ is generated in the gas phase and investigated with respect to both its structure and its reactivity toward small, inert molecules using Fourier-transform ion cyclotron resonance (FT-ICR) mass spectrometry and DFT-based calculations. $Al_2O_7^+$ reacts with CH_4 under ambient conditions via hydrogen atom transfer (HAT), and with H_2O a ligand exchange occurs which gives rise to the evaporation of two O_2 molecules. The resulting product ion $Al_2O_4H_2^+$ is also capable of abstracting a hydrogen atom from both H_2O and CH_4. As indicated in the $H_2O/2O_2$ ligand exchange and supported by collision-induced dissociation (CID) experiments, two O_2 units constitute structural elements of $Al_2O_7^+$. Further insight is provided by DFT calculations, performed at the unrestricted B3LYP/TZVP level, and reaction mechanisms are suggested on the basis of both the experimental and theoretical results.

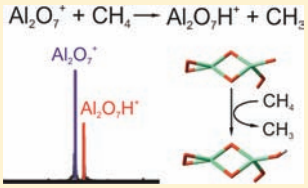

1. INTRODUCTION

As the principal component of natural gas, methane constitutes one of the largest hydrocarbon resources on earth, and activation of methane under ambient conditions to produce transportable liquids as well as more valuable chemicals has been identified as one of the key challenges in the context of addressing the global energy problem.[1,2] However, selective activation and functionalization of methane are not trivial, given the nature of the thermochemically strong (439 kJ mol^{-1})[3] and kinetically inert C−H bond.

Metal oxides are well established as catalysts for the activation of C−H bonds,[4] and aluminum oxides are also often used as supporting materials.[5−9] In addition, Al_2O_3 serves as one of the most active catalysts for D/H exchange in mixtures of D_2/CH_4 and CH_4/CD_4;[10] various aspects of the C−H bond activation processes have been extensively studied for γ-Al_2O_3.[4,11] Quite recently, the reactive sites of γ-Al_2O_3 have been identified in a combined experimental/computational study; it was found that the presence of a moderate coverage with water increases the number of reactive nonadjacent Al−O Lewis acid−base pairs.[12] However, the existing information on the precise nature and the detailed operation of the active sites is, for many catalytic systems, still rather limited.

A promising way to study, at a strictly molecular level, the active sites of metal oxides is to generate gas-phase metal oxide clusters and to examine their chemical reactivity.[13−22] In fact, previous studies have revealed that aluminum-containing gas-phase clusters exhibit quite unusual features. For example, rather interesting reactivity trends were reported in the oxidation of CO by $Al_2O_3^+$ and $Al_2O_{3,4}^-$ clusters.[23] The groups of Wang and Boldyrev determined in detailed spectroscopic studies the structures and bonding features of small aluminum-related clusters.[24−31] For example, they confirmed the experimentally observed coexistence of cagelike and sheetlike isomers for the $Al_4O_6^-$ cluster.[32] Bare and microsolvated anionic aluminum oxides have also been investigated by Neumark and co-workers[33] and by the Jarrold group,[34−36] both using photoelectron spectroscopy; according to these studies, two structural isomers of $Al_3O_3^-$ are observed and hydroxy complexes are generated by addition of water and methanol to $Al_3O_3^-$ and $Al_5O_4^-$. The combined IR spectroscopic/computational work of Asmis and co-workers revealed details about the canonical structures of $[(Al_2O_3)_x(AlO)]^+$ ($x = 1−4$) as well as of $[(Al_2O_3)_4]^+$ bearing a terminal Al−$O^\bullet$ single bond.[37,38] Feyel et al. demonstrated that $[(Al_2O_3)_x]^+$ cluster ions ($x = 3−5$) abstract a hydrogen atom from methane under thermal conditions; in distinct contrast, clusters having an odd number of aluminum atoms exhibit no activity toward methane.[39]

The striking cluster-size-dependent behavior of these aluminum oxide clusters toward methane was explained by the presence versus absence of a high spin density located at a terminal oxygen atom, which turned out to be crucial for thermal hydrogen-atom transfer (HAT).[14,15,39−41] In addition to aluminum oxide clusters, numerous gas-phase experiments, focusing on methane activation under ambient conditions, have been carried out and quite a few oxide clusters are indeed able to bring about thermal activation of methane; the systems studied not only include transition-metal-based oxide clusters such as MnO^+,[42] FeO^+,[40,43] CoO^+,[44] CuO^+,[45] TiO_2^+,[46] ZrO_2^+,[46] MoO_3^+,[47] OsO_4^+,[48,49] and

Received: July 6, 2011
Published: September 12, 2011

$V_4O_{10}^+$,[50] but also main-group-metal oxide clusters such as MO^+ (M = Mg,[51] Ca,[52] Sr,[52] Ba,[52] Ge,[53] Sn,[53] Pb[53,54]) as well as nonmetallic SO_2^+,[55,56] $P_4O_{10}^+$,[57−59] and binary oxide clusters such as $AlVO_4^+$,[60] $V_xP_yO_{10}^+$ ($x + y = 4$),[61,62] and $[V_2O_5(SiO_2)_x]^+$ ($x = 1-4$).[63] Common to all these clusters is that they are either oxygen poor or stoichiometric in their composition. Although C−H bond activation of butane by the oxygen-rich *anionic* cluster $Zr_2O_8^-$ was reported recently,[64] to the best of our knowledge, there have been no reports on the thermal activation of methane by an oxygen-rich *cationic* cluster in the gas phase.

Herein, we report the first example of room-temperature activation of methane (and other small molecules) by the oxygen-rich $Al_2O_7^+$ cluster.

2. EXPERIMENTAL AND COMPUTATIONAL METHODS

2.1. Experimental Details. The ion/molecule reactions were performed with a Spectrospin CMS 47X FT-ICR mass spectrometer equipped with an external ion source as described elsewhere.[65,66] In brief, $Al_2O_7^+$ is generated by laser ablation of an aluminum target using a Nd:YAG laser operating at 1064 nm in the presence of ~1% O_2 seeded in helium carrier gas. Using a series of potentials and ion lenses, the ions are transferred into the ICR cell, which is positioned in the bore of a 7.05 T superconducting magnet. After thermalization by pulses of argon (ca. 2×10^{-6} mbar) and mass selection using the FERETS ion-ejection protocol,[67] the reactions of mass-selected $Al_2O_7^+$ are studied by introducing the neutral reactants via leak valves. The purity of methane was 99.995%. The experimental second-order rate constants are evaluated assuming the pseudo first-order kinetic approximation after calibration of the measured pressure and acknowledgment of the ion gauge sensitivities.[68] For the thermalized cluster ions a temperature of 298 K is assumed.[68]

In CID experiments, the mass-selected ions of interest are accelerated by single-ion excitation and then collided with xenon as a buffer gas such that fragmentation occurs. Variation of the collision energy can be achieved by changing the excitation time. The ion-cyclotron energy, E_c,[69] is defined by eq 1

$$E_c = (\beta e V_{pp} t_{exc})^2/(128\gamma^2 m) \quad (1)$$

with the geometrical factor $\beta = 0.83$ of the ICR cell, the elementary charge e, the peak-to-peak voltage of the excitation plates $V_{pp} = 8.4$ eV, the radius of the cell $\gamma = 0.03$ m, and the ion's mass m. E_c is converted to the center-of-mass energy, E_{cm}, according to eq 2:

$$E_{cm} = (m_{Xe}E_c)/(m + m_{Xe}) \quad (2)$$

Here, m_{Xe} stands for the mass of the collision gas xenon. A pressure of $p(Xe) = 7 \times 10^{-9}$ mbar was applied in all CID experiments with a collision time of 500 ms.

The well-established ion-cyclotron double-resonance (DR) technique[70] was used to identify the precursor ions of secondary or higher-order products. $^{18}O_2$ labeling experiments were carried out either by labeling the oxide-cluster ions employing $^{18}O_2$ seeded in He or by leaking $^{18}O_2$ directly into the ICR cell as a reactant. The purities of CD_4, CH_2D_2, and $^{18}O_2$ amount to 99 atom % D, 98 atom % D, and 97 atom % ^{18}O, respectively; all compounds were purchased from Sigma-Aldrich.

2.2. Computational Details. DFT calculations were performed using the Gaussian 09 program[71] employing the hybrid B3LYP exchange-correlation functional[72−74] with the unrestricted Kohn−Sham solution[75] and TZVP basis sets.[76] The unrestricted B3LYP/TZVP level of theory proved to be reliable in previous studies of cationic,[50,77−80] anionic,[81,82] and neutral[83−85] transition-metal oxide clusters and main-group-metal oxide clusters such as MgO^+,[51,86] $(Al_2O_3)_x^+$ ($x = 3-5$),[39] and $P_4O_{10}^+$,[58] as well as binary clusters such as $AlVO_4^+$,[60] $AlVO_5^-$,[87] $V_2SiO_8^-$,[88] $V_2SiO_7^+$,[63] and $V_3PO_{10}^+$[61,62] in their gas-phase reactions with small hydrocarbons. For the optimization of transition structures (TS), we employed either the Berny algorithm[89] or the synchronous transit-guided quasi-Newton (STQN) method.[90] For most cases, initial guess structures of the transition structures were obtained by relaxed potential-energy surface (PES) scans using an appropriate internal coordinate. Vibrational frequencies were calculated to characterize the nature of the stationary points as minima or transition structures; the relative energies (given in kJ mol^{-1}) were corrected for zero-point energy (ZPE) contributions. Intrinsic reaction coordinate (IRC) calculations[91−94] were also performed to connect the TS with the local minima. The computation of Mulliken spin densities with the B3LYP method has been proven to provide reliable results in comparison with other theoretical methods[95] such as natural bond orbitals (NBO) or atoms in molecules (AIM); the approach also performed sufficiently well in comparison with the experimentally derived polarized neutron diffraction (PND) data of several transition-metal complexes.[95,96]

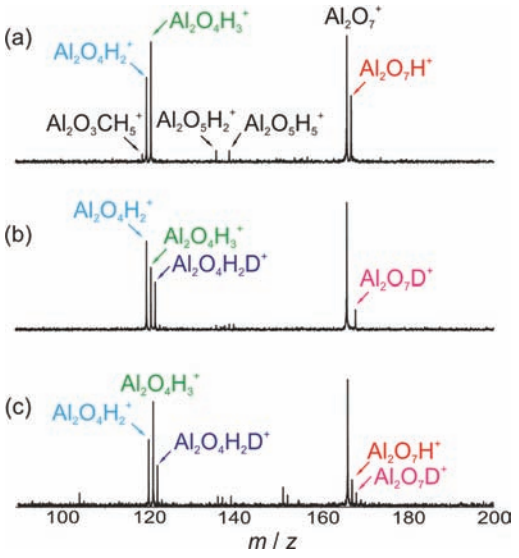

Figure 1. Mass spectra for the thermal reactions of $Al_2O_7^+$ with (a) CH_4 at a pressure of ca. 2×10^{-7} mbar after a reaction time of 15 s, (b) CD_4 at a pressure of ca. 2×10^{-7} mbar after a reaction time of 15 s, (c) CH_2D_2 at a pressure of ca. 4×10^{-7} mbar after a reaction time of 8 s.

3. RESULTS AND DISCUSSION

3.1. Experimental Results. *3.1.1. Primary Reactions of $Al_2O_7^+$ with CH_4 and H_2O.* When mass-selected, thermalized $Al_2O_7^+$ ions are exposed to CH_4 or H_2O in the ICR cell, three main product ions, i.e. $Al_2O_7H^+$, $Al_2O_4H_2^+$, and $Al_2O_4H_3^+$, are formed (Figure 1a); the first two ions originate from reactions 3 and 4, respectively (Figure S1); the last one corresponds to a secondary process and is discussed further below. The overall rate constant $k(Al_2O_7^+ + CH_4/H_2O)$ is determined to be 8.1×10^{-12} cm^3 s^{-1} $molecule^{-1}$ with an uncertainty of ±50%; this amounts to a collision efficiency of 1%. According to the DFT calculations, for reactions 3 and 4 the zero-point energy corrected reaction energies, ΔE, are rather exothermic (Gibbs free energies ΔG at 298 K are given in parentheses).

$$Al_2O_7^+ + CH_4 \rightarrow Al_2O_7H^+ + CH_3$$
$$\Delta E = -102 \text{ kJ mol}^{-1} (\Delta G = -103 \text{ kJ mol}^{-1}) \quad (3)$$

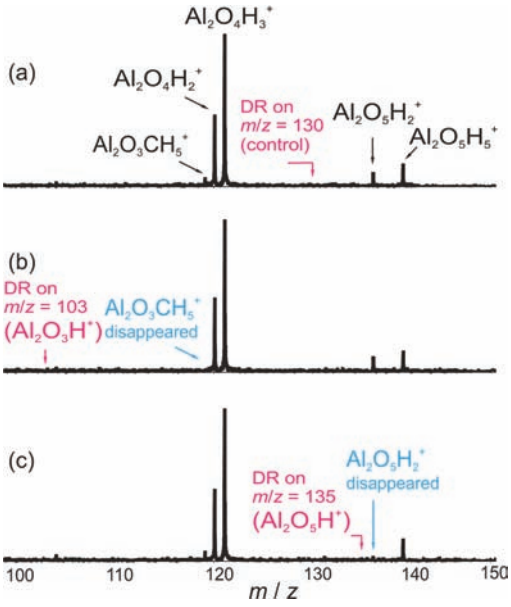

Figure 2. Double-resonance (DR) experiments: (a) reference spectrum with DR on m/z 130 as a control experiment; (b, c) DR on the putative intermediates (b) $Al_2O_3H^+$ and (c) $Al_2O_5H^+$, resulting in the disappearance of the signals for $Al_2O_3CH_5^+$ and $Al_2O_5H_2^+$, respectively. The reaction time amounts to 20 s for all of the spectra at a methane pressure of 2×10^{-7} mbar.

$$Al_2O_7^+ + H_2O \rightarrow Al_2O_4H_2^+ + 2O_2$$
$$\Delta E = -127 \text{ kJ mol}^{-1} (\Delta G = -164 \text{ kJ mol}^{-1}) \quad (4)$$

The HAT and the $H_2O/2O_2$ exchange have been further confirmed by labeling experiments. Using CD_4 and CH_2D_2 as substrates (Figure 1b,c), the product ions $Al_2O_7D^+$ and $Al_2O_7H^+/Al_2O_7D^+$ are formed, respectively (eqs 5 and 6). $Al_2O_4H_2^+$ must originate from a reaction of $Al_2O_7^+$ with background water that is present in the ICR mass spectrometer, since neither $Al_2O_4D_2^+$ nor $Al_2O_4HD^+$ are generated. The intramolecular kinetic-isotope effect (KIE = k_{C-H}/k_{C-D}) as determined from the branching ratios of reactions 6a and 6b amounts to 1.9. As expected, the reaction of $Al_2{}^{18}O_7^+$ with background $H_2{}^{16}O$ results in the formation of a product ion with m/z 126 corresponding to $Al_2{}^{18}O_3{}^{16}OH_2^+$ (eq 7).

$$Al_2O_7^+ + CD_4 \rightarrow Al_2O_7D^+ + CD_3 \quad (5)$$

$$Al_2O_7^+ + CH_2D_2 \rightarrow Al_2O_7H^+ + CHD_2 \quad (6a)$$

$$\rightarrow Al_2O_7D^+ + CH_2D \quad (6b)$$

$$Al_2{}^{18}O_7^+ + H_2{}^{16}O \rightarrow Al_2{}^{18}O_3{}^{16}OH_2^+ + 2{}^{18}O_2 \quad (7)$$

3.1.2. Secondary Reactions. As revealed by high-resolution measurements, the signals at m/z 119, 121, 136, and 139 in Figure 1a correspond to $Al_2O_3CH_5^+$, $Al_2O_4H_3^+$, $Al_2O_5H_2^+$, and $Al_2O_5H_5^+$, respectively. These ions are formed in secondary (or higher order) reactions, and the individual reaction sequences are revealed by double-resonance experiments in which labeled as well as unlabeled substrates have been employed (see Figure S2). Once more, on the basis of the DFT calculations, reactions 8−10 are quite exothermic.

Scheme 1. Reaction Pathways Determined for the $Al_2O_7^+/CH_4/H_2O$ System[a]

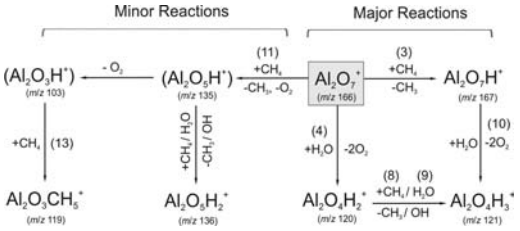

[a] While $Al_2O_3H^+$ and $Al_2O_5H^+$ are not observed, they have been identified as intermediates in DR experiments. For details, see text.

$$Al_2O_4H_2^+ + CH_4 \rightarrow Al_2O_4H_3^+ + CH_3$$
$$\Delta E = -91 \text{ kJ mol}^{-1} (\Delta G = -94 \text{ kJ mol}^{-1}) \quad (8)$$

$$Al_2O_4H_2^+ + H_2O \rightarrow Al_2O_4H_3^+ + OH$$
$$\Delta E = -45 \text{ kJ mol}^{-1} (\Delta G = -44 \text{ kJ mol}^{-1}) \quad (9)$$

$$Al_2O_7H^+ + H_2O \rightarrow Al_2O_4H_3^+ + 2O_2$$
$$\Delta E = -116 \text{ kJ mol}^{-1} (\Delta G = -153 \text{ kJ mol}^{-1}) \quad (10)$$

While the formation of $Al_2O_5H_5^+$ has been traced back to the addition of water to $Al_2O_4H_3^+$, for the ion $Al_2O_4H_3^+$, three independent consecutive pathways have been identified: i.e. the combinations of eqs 3/10, eqs 4/8, and eqs 4/9, respectively. Regarding the possible precursors for the generation of $Al_2O_3CH_5^+$ and $Al_2O_5H_2^+$, some of the conceivable transient intermediates have indeed been identified. For example, when the precursor ion $Al_2O_5H^+$ is subjected to DR, the signal for $Al_2O_5H_2^+$ is diminished (Figure 2c): i.e. $Al_2O_5H^+$ serves as an intermediate that reacts in a secondary reaction with a hydrogen atom source (most likely H_2O or CH_4) to generate $Al_2O_5H_2^+$. $Al_2O_5H^+$ itself is produced from $Al_2O_7^+$ (eq 11), and this process has been calculated to be exothermic by −78 kJ mol^{-1}. Obviously, the calculated bond energies of both BDE($Al_2O_5^+-O_2$) = 30 kJ mol^{-1} and BDE($Al_2O_5H^+-O_2$) = 24 kJ mol^{-1} are much smaller as compared to the reaction energy liberated in the HAT (eq 3).

$$Al_2O_7^+ + CH_4 \rightarrow Al_2O_5H^+ + CH_3 + O_2$$
$$\Delta E = -78 \text{ kJ mol}^{-1} (\Delta G = -116 \text{ kJ mol}^{-1}) \quad (11)$$

Next, the continuous ejection of $Al_2O_3H^+$ from the ICR cell annihilates the signal corresponding to $Al_2O_3CH_5^+$ (Figure 2b). Thus, $Al_2O_3H^+$ serves as an intermediate which reacts further in a secondary process according to eq 13. The formation of $Al_2O_3H^+$, according to eq 12, has been calculated to be endothermic by 65 kJ mol^{-1}; however, this process is exergonic with a Gibbs free energy of −11 kJ mol^{-1} when the contribution of entropy is taken into account. The large contribution of entropy for this reaction is reasonable, since four products are formed from two

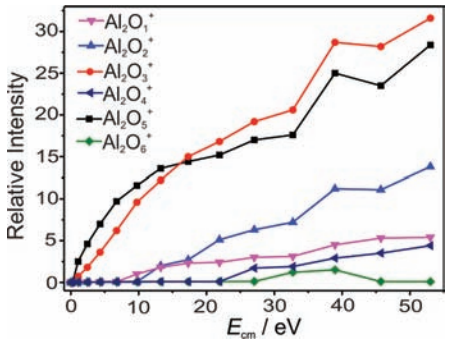

Figure 3. CID of $Al_2O_7^+$ with center-of-mass energies (E_{cm}) in the range 0−60 eV.

reactant molecules.

$$Al_2O_7^+ + CH_4 \rightarrow Al_2O_3H^+ + CH_3 + 2O_2 \quad \Delta E = 65\ \text{kJ mol}^{-1}\ (\Delta G = -11\ \text{kJ mol}^{-1}) \tag{12}$$

$$Al_2O_3H^+ + CH_4 \rightarrow Al_2O_3CH_5^+ \quad \Delta E = -136\ \text{kJ mol}^{-1}\ (\Delta G = -105\ \text{kJ mol}^{-1}) \tag{13}$$

The complete reactivity network of the $Al_2O_7^+/CH_4/H_2O$ system is summarized in Scheme 1.

3.1.3. Structure of $Al_2O_7^+$. Reaction 4 implies that there exist two loosely bound O_2 moieties in $Al_2O_7^+$. To verify this assumption further, we carried out CID experiments[69] (Figure 3). At a collision energy E_{cm} < 10 eV, O_2 elimination(s) to form $Al_2O_5^+$ and $Al_2O_3^+$, respectively, are observed exclusively. On an increase of E_{cm} from 10 to 20 eV, $Al_2O_2^+$ and Al_2O^+ are generated additionally, in which the loss of atomic oxygen takes place. At even higher energies (E_{cm} > 20 eV), one observes a signal for $Al_2O_6^+$, which results from the direct loss of one O atom from $Al_2O_7^+$. As shown in Figure 3, there exists a significant energy gap between the elimination of one and two O_2 molecules versus the fragmentation pathways which involve O atom losses; there observations further underline the presence of two O_2 moieties in $Al_2O_7^+$.

Since the CID experiments (in line with the facile ligand exchange of $2O_2$ for H_2O; eq 4) indicate the presence of two loosely bound O_2 moieties in $Al_2O_7^+$, an $^{16}O_2/^{18}O_2$ exchange is expected to take place efficiently.[97−100] However, when $^{18}O_2$ is leaked into the ICR reaction cell, no product species $Al_2{}^{16}O_{7-x}{}^{18}O_x^+$ (x = 2, 4) indicative of an $^{16}O_2/^{18}O_2$ exchange are observed; this finding is quite surprising and—neglecting KIEs—can only be explained by a barrier for the $^{16}O_2/^{18}O_2$ exchange processes, the origin of which remains unknown for the time being.

3.2. DFT Results. Figure 4 summarizes the DFT optimized geometries of $Al_2O_xH_y^+$ (x = 3, 5, 7; y = 0, 1) and $Al_2O_4H_y^+$ (y = 2, 3); these species are relevant in the present context. Next, the structural and electronic properties of these cluster cations will be discussed.

3.2.1. Oxide Clusters $Al_2O_3^+$, $Al_2O_5^+$, and $Al_2O_7^+$. All three binary aluminum-oxide cluster cations in their most stable structures possess terminal, oxygen-centered radicals. Throughout the following discussion, the aluminum atom bearing the terminal oxygen is denoted as Al(2) and the remaining Al atoms are denoted as Al(1). Among the numerous conceivable isomers,

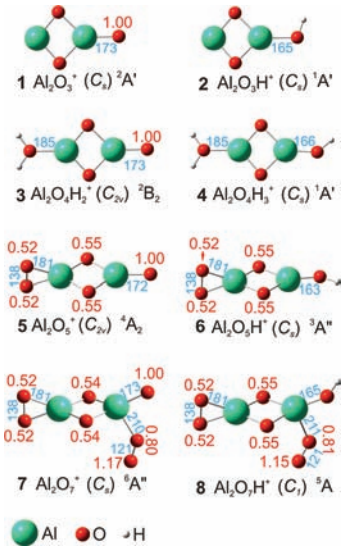

Figure 4. Calculated structures suggested to act as the key species in the experiments. Mulliken-spin-density values are denoted in red, and key bond lengths (in pm) are given in blue. Charges have been omitted for the sake of clarity.

the proposed structures for $Al_2O_5^+$ (**5**) and $Al_2O_7^+$ (**7**) are inspired by the CID experiments, which indicate the presence of one and two loosely bound O_2 moieties, respectively. Thus, the most stable structure for $Al_2O_5^+$ is obtained by adding one O_2 unit side-on to the less coordinated Al(1) atom of $Al_2O_3^+$. In addition to the unpaired electron located at the terminal oxygen (denoted as O_t), for the quartet ground state of $Al_2O_5^+$ two unpaired electrons are almost equally distributed over the η^2-O_2 moiety and the two bridging oxygen atoms (denoted as O_b). Side-on-bound η^2-superoxo units have also been described for gaseous $V_2O_6^+$.[101] Further, adding one more O_2 molecule to $Al_2O_5^+$ results in the formation of $Al_2O_7^+$, in which, however, O_2 is most favorably bound in an end-on fashion to the Al(2) atom. In **7**, the calculated O−O bond distance of the newly formed ligand amounts to 120.7 pm, which is almost the same as the distance in free O_2 (120.8 pm); thus, the calculation suggests the generation of a genuine O_2 complex in the experiments. The bond dissociation energy for the reaction **7** → **5** + O_2, i.e. BDE($Al_2O_5^+$−O_2), is calculated to amount to only 30 kJ mol^{-1} at the B3LYP/TZVP level of theory. Note that the addition of a second O_2 moiety to $Al_2O_5^+$ to form $Al_2O_7^+$ does not affect the presence of a terminal oxygen-centered radical at $O_t^{\bullet}$.

Mulliken atom spin density (MASD) analyses on $^6Al_2O_7^+$ (**7**) indicate a hole that is symmetrically delocalized over the two bridging oxygen atoms. Spin delocalization over bridged oxygen atoms bound to Al or Mg centers, respectively, has been described in the literature before. While it has been noted that spin delocalization over four O atoms in models for α-quartz $[AlO_4]^0$ centers are overestimated by pure DFT functionals and are thus artificial,[102] the picture of spin delocalization for $Mg_2O_2^+$ obtained at the B3LYP and CCSD(T) levels of theory has been confirmed by IR multiphoton-dissociation experiments.[103] The bias for delocalization by DFT theory has been attributed to a nonexact treatment of the electron-exchange energy; hence, the self-interaction is not completely canceled out as in HF calculations and the overestimated Coulomb repulsion can be reduced by delocalization. Thus, when using for example the BHLYP or

BB1K functionals having larger Hartree-Fock (HF) exchange terms (50% and 44%, respectively), the electron hole is localized only on a single oxygen for the aluminum systems;[104] the same picture emerges in HF and HF-LYP calculations using 100% exact exchange, and the EPR hyperfine coupling parameters computed in these calculations are in line with experimental data.[105] In contrast, a higher mixing of up to 50% HF exchange does not change the spin distribution of $Mg_2O_2^+$; here, a symmetric hole delocalization over the two bridging oxygen atoms, as obtained by B3LYP, is reproduced.[106] The same holds true for $Al_2O_7^+$ investigated in this study: When a higher percentage of electron exchange of up to 50% is employed by using the BHLYP functional, spin delocalization over the two bridging oxygen atoms in $Al_2O_7^+$ is preserved.

With regard to the multiplicity of $Al_2O_7^+$, the doublet, quartet, and sextet states are almost isoenergetic with relative energies of 0.3, 0.6, and 0.0 kJ mol^{-1}, respectively. The calculated $\langle S^2\rangle$ values for $^4Al_2O_7^+$ and $^2Al_2O_7^+$ (4.77 and 2.78, respectively) are higher than the expected $\langle S^2\rangle$ values (3.75 and 0.75, respectively); this points to broken-symmetry characters of these two states.[78,107,108] As described above for $^4Al_2O_7^+$, an electron hole is symmetrically delocalized over the two bridging oxygen atoms in $^4Al_2O_7^+$ which are antiferromagnetically coupled to the unpaired electron localized at the terminal side-on η^2-O_2 unit. Finally, a spin flip of the latter leads to $^2Al_2O_7^+$, as indicated by the MASD analysis (Figure S3). Furthermore, the natural population analysis (NPA) charge distributions of $^4Al_2O_7^+$ and $^2Al_2O_7^+$ are exactly the same as that for $^6Al_2O_7^+$ (**7**) (see also Figure S3). All these features strongly suggest that the calculated $^4Al_2O_7^+$ and $^2Al_2O_7^+$ spin states are actually broken-symmetry states. According to the broken-symmetry approach,[78,107−109] the Heisenberg exchange coupling constant J can be calculated from the energies of the broken-symmetry state and the highest pure spin multiplet. The J values of $Al_2O_7^+$ are positive; thus, the conventional quartet and doublet states are higher in energy in comparison to the sextet state.

For $^6Al_2O_7^+$, two additional structural isomers (structures **S2** and **S3** in Figure S4) have been obtained; for both, a similar bonding situation exists with one oxygen-centered radical as well as two O_2 units. **S2** and **S3** are only 12 and 15 kJ mol^{-1} higher in energy than **7**, respectively. Structure **7** is connected with **S2** via an isomerization barrier of 20 kJ mol^{-1}; however, it was not possible to locate a barrier for the **S2** → **S3** isomerization, due to a very flat PES at this region. Further, the reactions of these three isomers with CH_4 and H_2O have been calculated to be rather similar with respect to the exothermicities and the barriers involved; thus, the overall reaction pattern does not change. For two additional $Al_2O_7^+$ isomers (structures **S5** and **S6** in Figure S4) we obtain peroxide-bridged structures bearing an Al−O−O−Al moiety; however, as these structures are 82 and 166 kJ mol^{-1} higher in energy than that of **7**, we do not expect them to be generated in the experiments.

3.2.2. Hydroxide Clusters $Al_2O_3H^+$, $Al_2O_5H^+$, and $Al_2O_7H^+$. HAT from methane by $Al_2O_7^+$ to form $Al_2O_7H^+$ involves the terminal oxygen atom bearing an unpaired electron. We also considered computationally the formation of the isomer $[Al_2O_5(OOH)]^+$ that would contain a hydroperoxide ligand; this product complex can be generated by HAT from CH_4 to the end-on bound O_2 moiety, which possesses a spin density value of 1.15 at the distal oxygen atom. However, formation of $[Al_2O_5(OOH)]^+ + CH_3$ is 117 kJ mol^{-1} higher in energy as compared to the entrance channel of $Al_2O_7^+ + CH_4$. This finding is not surprising, given the fact that the end-on-bound O_2 unit in **7** corresponds to an almost undisturbed $^3O_2$ molecule; in line with this, HAT from methane by free $^3O_2$ has been calculated to be endothermic by 230 kJ mol^{-1}. The hydroxide clusters $Al_2O_3H^+$ and $Al_2O_5H^+$ are related to $Al_2O_7H^+$ in terms of removing two or one O_2 units, respectively, from the latter. Since $Al_2O_3^+$ and $Al_2O_5^+$ also possess an unpaired electron at a terminal oxygen (see above), HAT from methane is expected to occur also for these cations. While $Al_2O_5^+$ has not been investigated due to low intensities, $Al_2O_3^+$ reacts with methane under HAT and formaldehyde formation with a much higher efficiency;[110] thus, the two O_2 molecules in $Al_2O_7^+$ cause a higher selectivity at the expense of efficiency.

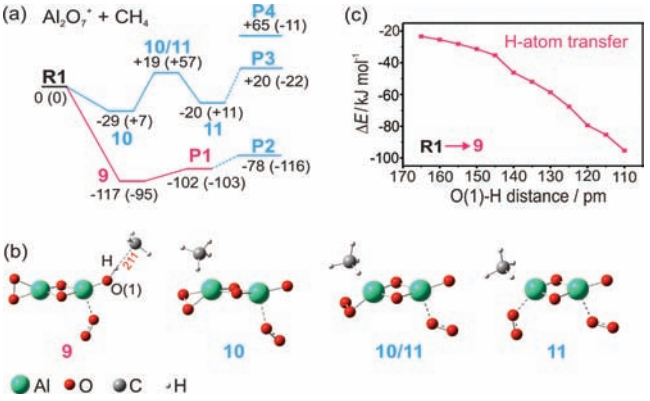

Figure 5. (a) Sextet PES (in kJ mol^{-1}) for the reaction of $Al_2O_7^+$ with CH_4, as calculated at the unrestricted B3LYP/TZVP level of theory: **R1** = $Al_2O_7^+ + CH_4$; **P1** = $Al_2O_7H^+ + CH_3$; **P2** = $Al_2O_5H^+ + CH_3 + O_2$; **P3** = $[Al_2O_3(CH_4)]^+ + 2O_2$; **P4** = $Al_2O_3H^+ + CH_3 + 2O_2$. The relative energies ΔE (ΔG values are given in parentheses) are related to the $Al_2O_7^+/CH_4$ entrance channel and are given in kJ mol^{-1}. (b) Fully optimized structures of intermediates **9**−**11** and transition structure **10**/**11**. Cartesian coordinates are available as Supporting Information. (c) Relaxed scan of the O−H distance during the HAT from methane by $Al_2O_7^+$.

3.2.3. Cluster Ions $Al_2O_4H_2^+$ and $Al_2O_4H_3^+$. Formation of the ion $Al_2O_4H_2^+$ according to reaction 4 most likely results in the generation of the cluster $[Al_2O_3(H_2O)]^+$ (**3**), which contains an intact H_2O molecule connected to the less coordinated Al(1) atom of $Al_2O_3^+$. Although the generation of the isomeric hydroxide cluster $[Al_2O_2(OH)_2]^+$ (C_s) with two hydroxide ligands bound to each Al atom is more favored by 183 kJ mol^{-1} (see Figure S5), its formation would require a much more complex reaction sequence. However, unambiguous structural information about the product ion generated in reaction 4 cannot be given for the time being. Also, the exothermic formation of the secondary product $Al_2O_4H_3^+$ according to reactions 8 and 9 (−91 and −45 kJ mol^{-1}, respectively) can be attributed to either the water complex $[Al_2O_3(H_2O)]^+$ or the hydroxide cluster $[Al_2O_2(OH)_2]^+$; both species might then react consecutively with water or methane, respectively, to generate the product complex $[Al_2O_2(OH)(H_2O)]^+$, bearing a hydroxo and a water ligand. The relative energy of $Al_2O_4H_2^+$ (C_{2v}) has been employed in calculating the PES of $Al_2O_7^+ + H_2O$ and $Al_2O_4H_2^+ + CH_4$.

3.2.4. Mechanism of the HAT: $Al_2O_7^+ \rightarrow Al_2O_7H^+$. DFT calculations have been conducted to obtain mechanistic insight into the ion/molecule reactions of $Al_2O_7^+$ with CH_4 (Figure 5a,b). As for $Al_2O_7^+$, the sextet state of the intermediates and transition states involved in this reaction are lower in energy compared to

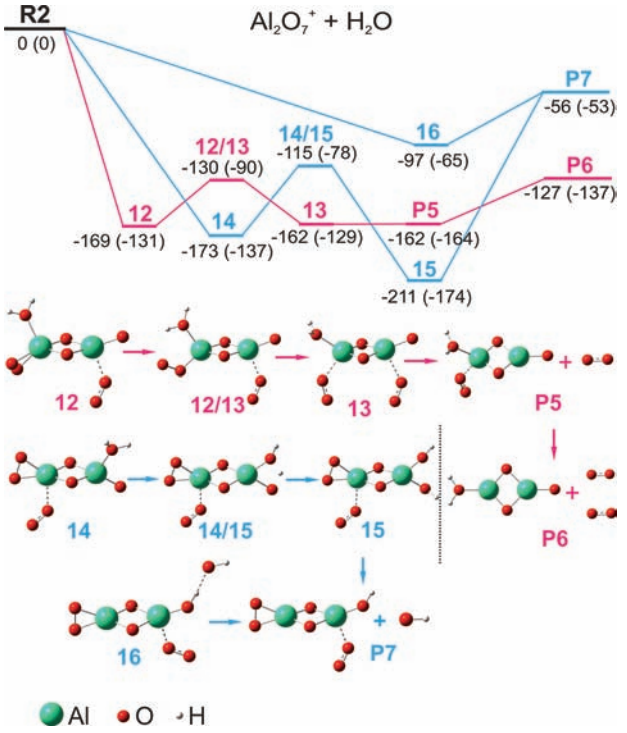

Figure 6. Ion/molecule reactions of $Al_2O_7^+$ with H_2O on the sextet PES with fully optimized structures of the intermediates and transition structures as calculated at the unrestricted B3LYP/TZVP level of theory: **R2** = $Al_2O_7^+ + H_2O$; **P5** = $[Al_2O_5(H_2O)]^+ + O_2$; **P6** = $[Al_2O_3(H_2O)]^+ + 2O_2$; **P7** = $Al_2O_7H^+ + OH$. The relative energies ΔE (ΔG values are given in parentheses) are given in kJ mol^{-1}. Cartesian coordinates are available as Supporting Information.

the quartet and doublet states according to the broken-symmetry approach; thus, only the sextet PES is considered. The calculated PES for the HAT in the $Al_2O_7^+/CH_4$ system, conducted at the unrestricted B3LYP/TZVP level, reveals some subtle differences when compared with, for example, the $Al_8O_{12}^+/CH_4$ system. For the latter it had been found that the reaction proceeds via the encounter complex $Al_8O_{12}^+\cdots CH_4$, in which one hydrogen atom interacts weakly with the radical center of the oxygen atom ($\Delta E = -10$ kJ mol^{-1}).[39] In contrast, for the $Al_2O_7^+/CH_4$ system we note that the HAT proceeds in a barrierless fashion to generate directly the intermediate $Al_2O_7H^+\cdots CH_3$ (**9**) (Figure 5c); despite several attempts, no encounter complex of the type $Al_2O_7^+\cdot CH_4$ has been located on the PES. In intermediate **9**, the CH_3 moiety is loosely coordinated to the hydrogen atom of the newly formed hydroxy ligand with an $(Al_2O_6)OH^+\cdots CH_3$ distance of 211 pm. The HAT is completed by loss of a methyl radical concomitant with the formation of $Al_2O_7H^+$ as the ionic product. This kind of a smooth, direct HAT is rather similar to those calculated for the $P_{4-x}V_xO_{10}^+/CH_4$ ($x = 0, 2-4$)[50,58,61,62] and $AlVO_4^+/CH_4$ systems.[60] Another possible reaction pathway for $Al_2O_7^+ + CH_4$ has also been considered; here, CH_4 is adsorbed to Al(2), resulting in the evaporation of two O_2 units (**R1** → **10** → **10/11** → **11** → **P2**). However, TS **10/11** is 19 kJ mol^{-1} higher in energy compared to the entrance channel; in line with this, no CH_4/O_2 ligand exchange is observed in the experiments.

3.2.5. Reactions of $Al_2O_7^+$ with H_2O. The ligand-exchange with water according to eq 4 is also observed without leaking neutral H_2O into the ICR cell and can be traced back to reactions

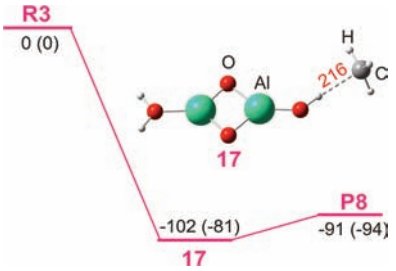

Figure 7. Ion/molecule reaction of $[Al_2O_3(H_2O)]^+$ with CH_4 on the doublet PES: **R3** = $[Al_2O_3(H_2O)]^+$ (**3**) + CH_4; **P8** = $[Al_2O_3H(H_2O)]^+$ (**4**) + CH_3. The energies ΔE (ΔG values are given in parentheses) are given related to the initial reactants (in kJ mol^{-1}).

of $Al_2O_7^+$ with residual water present in the instrument ($<1.5 \times 10^{-9}$ mbar). This exchange is the only primary reaction of $Al_2O_7^+$ with water; O−H bond activation of the latter does not play a role.

However, HAT from water to generate a hydroxyl radical according to eq 14 has been calculated to be exothermic by −56 kJ mol^{-1} on the sextet PES.[111] As shown in Figure 6, the formation of $Al_2O_7H^+$ and OH can proceed via two different pathways. The first one corresponds to a direct HAT in which intermediate **16** is formed without any barrier, in analogy to the HAT from methane to a terminal oxygen of $Al_2O_7^+$. In the second reaction channel, H_2O is coordinated to Al(2) prior to the O−H bond-activation reaction; this pathway then proceeds via the sequence **14** → **14/15** → **15** → $Al_2O_7H^+ + OH$, as depicted in blue in Figure 6.

$$Al_2O_7^+ + H_2O \rightarrow Al_2O_7H^+ + OH \quad (14)$$
$$\Delta E = -56 \text{ kJ mol}^{-1} \ (\Delta G = -53 \text{ kJ mol}^{-1})$$

The reason that HAT(eq 14) is not observed in the experiment might be due to the fact that the competing loss of two molecules of oxygen according to eq 4 not only is much more exothermic but also is entropically favored. Depending on the order of the O_2 loss from Al(1) and Al(2), respectively, several alternative reaction paths for the release of two O_2 molecules are accessible, with transition structures and intermediates being similar in energy; one representative example of these reaction sequence is depicted in Figure 6 proceeding along the sequence **12** → **12/13** → **13** → $[Al_2O_5(H_2O)]^+ + O_2 \rightarrow [Al_2O_3(H_2O)]^+ + 2O_2$.

3.2.6. Reaction of $[Al_2O_3(H_2O)]^+$ with CH_4. The C_{2v} isomer of $Al_2O_4H_2^+$ (**3**) possesses a spin located at a terminal Al−O$^\bullet$ moiety. DFT calculations are performed for the ion/molecule reactions of $[Al_2O_3(H_2O)]^+$ with CH_4 on the doublet PES (Figure 7). The coordination of methane to $[Al_2O_3(H_2O)]^+$ and the smooth HAT are associated with a significant gain of energy (−102 kJ mol^{-1}). As in the $Al_2O_7^+/CH_4$ system, no encounter complex $[Al_2O_3(H_2O)]^+\cdots CH_4$ could be located on the PES; instead, the calculations suggest the formation of the intermediate $[Al_2O_2(H_2O)OH]^+\cdots CH_3$ during the structure optimizations, which implies that the reaction proceeds without a noticeable reaction barrier by a direct HAT.

4. CONCLUSIONS

The oxygen-rich cluster cation $Al_2O_7^+$ has been generated in the gas phase, and its thermal reactions with CH_4 and H_2O were probed using FT-ICR mass spectrometry and analyzed by means of DFT calculations. $Al_2O_7^+$ is able to abstract a hydrogen atom

from methane at room temperature; according to the DFT calculations a terminal oxygen atom which possesses an unpaired electron constitutes the active site in the encounter complex. In the reaction of $Al_2O_7^+$ with background water present in the reaction cell, a ligand exchange reaction according to $Al_2O_7^+ + H_2O \rightarrow Al_2O_4H_2^+ + 2O_2$ is observed; the presence of two O_2 units in $Al_2O_7^+$ is corroborated by CID experiments. The primary product $Al_2O_4H_2^+$ subsequently also reacts with either H_2O or CH_4 by HAT to generate $Al_2O_4H_3^+$.

To the best of our knowledge, HAT from methane by $Al_2O_7^+$ constitutes the first example of thermal activation of CH_4 by a cationic, oxygen-rich metal cluster.

■ ASSOCIATED CONTENT

Supporting Information. Complete ref 71; isosurface plots showing the spin distributions on calculated sextet, quartet, and doublet $Al_2O_7^+$, DR mass spectra, DFT optimized isomer geometries of $Al_2O_7^+$ and $Al_2O_4H_2^+$, and Cartesian coordinates for all optimized structures. This material is available free of charge via the Internet at http://pubs.acs.org.

■ AUTHOR INFORMATION

Corresponding Author

*Maria.Schlangen@mail.chem.tu-berlin.de (M.S.); Helmut.Schwarz@mail.chem.tu-berlin.de and HSchwarz@kau.edu.sa (H.S.).

■ ACKNOWLEDGMENT

This work is supported by the Fonds der Chemischen Industrie, the Deutsche Forschungsgemeinschaft, and the cluster of excellence "Unifying Concepts in Catalysis" (coordinated by the Technische Universität Berlin and funded by the DFG). For computational resources, the Institut für Mathematik at the Technische Universität Berlin is acknowledged. We thank Burkhard Butschke, Nicolas Dietl, Robert Müller, Johannes Schraut, and Dr. Detlef Schröder, as well as Prof. Xunlei Ding, for helpful suggestions and discussions. Z.-C.W. is grateful to the Alexander von Humboldt-Stiftung for a postdoctoral fellowship. R.K. acknowledges the Stiftung Stipendien Fonds des Verbandes der Chemischen Industrie for a Kékulé scholarship. We dedicate this publication to the memory of Carl Bosch.

■ REFERENCES

(1) Webb, J. R.; Bolaño, T.; Gunnoe, T. B. *ChemSusChem* **2011**, *4*, 37.
(2) Olah, G. A.; Goeppert, A.; Prakash, G. K. S. *Beyond Oil and Gas: The Methanol Economy*; Wiley-VCH: Weinheim, Germany, 2009.
(3) Berkowitz, J.; Ellison, G. B.; Gutman, D. *J. Phys. Chem.* **1994**, *98*, 2744.
(4) Copéret, C. *Chem. Rev.* **2010**, *110*, 656.
(5) Lewandowska, A. E.; Banares, M. A.; Khabibulin, D. F.; Lapina, O. B. *J. Phys. Chem. C* **2009**, *113*, 20648.
(6) Fortrie, R.; Todorova, T. K.; Ganduglia-Pirovano, M. V.; Sauer, J. *J. Chem. Phys.* **2008**, *129*, 224710.
(7) Todorova, T. K.; Ganduglia-Pirovano, M. V.; Sauer, J. *J. Phys. Chem. B* **2005**, *109*, 23523.
(8) Döbler, J.; Pritzsche, M.; Sauer, J. *J. Am. Chem. Soc.* **2005**, *127*, 10861.
(9) Brazdova, V.; Ganduglia-Pirovano, M. V.; Sauer, J. *J. Phys. Chem. B* **2005**, *109*, 23532.
(10) Larson, J. G.; Hall, W. K. *J. Phys. Chem.* **1965**, *69*, 3080.
(11) Joubert, J.; Salameh, A.; Krakoviack, V.; Delbecq, F.; Sautet, P.; Copéret, C.; Basset, J. M. *J. Phys. Chem. B* **2006**, *110*, 23944.
(12) Wischert, R.; Copéret, C.; Delbecq, F.; Sautet, P. *Angew. Chem., Int. Ed.* **2011**, *50*, 3202.
(13) Schwarz, H. *Angew. Chem., Int. Ed.* **2011**, DOI: 10.1002/anie.201006424, and references therein.
(14) Schlangen, M.; Schwarz, H. *J. Chem. Soc., Dalton Trans.* **2009**, *46*, 10155.
(15) Schröder, D.; Schwarz, H. *Proc. Natl. Acad. Sci. U.S.A.* **2008**, *105*, 18114.
(16) Böhme, D. K.; Schwarz, H. *Angew. Chem., Int. Ed.* **2005**, *44*, 2336.
(17) Schwarz, H.; Schröder, D. *Pure. Appl. Chem.* **2000**, *72*, 2319.
(18) Schröder, D.; Schwarz, H. *Angew. Chem., Int. Ed.* **1995**, *34*, 1973.
(19) Schwarz, H. *Angew. Chem., Int. Ed.* **1991**, *30*, 820.
(20) Johnson, G. E.; Mitrić, R.; Bonačić-Koutecký, V.; Castleman, A. W., Jr. *Chem. Phys. Lett.* **2009**, *475*, 1.
(21) Roithová, J.; Schröder, D. *Chem. Rev.* **2010**, *110*, 1170.
(22) Johnson, G. E.; Tyo, E. C.; Castleman, A. W., Jr. *Proc. Natl. Acad. Sci. U.S.A.* **2008**, *105*, 18108.
(23) Johnson, G. E.; Tyo, E. C.; Castleman, A. W., Jr. *J. Phys. Chem. A* **2008**, *112*, 4732.
(24) Desai, S. R.; Wu, H. B.; Rohlfing, C. M.; Wang, L. S. *J. Chem. Phys.* **1997**, *106*, 1309.
(25) Li, X.; Wang, L. S.; Cannon, N. A.; Boldyrev, A. I. *J. Chem. Phys.* **2002**, *116*, 1330.
(26) Li, X.; Wang, L. S. *Phys. Rev. B: Condens. Matter Mater. Phys.* **2002**, *65*, 153404.
(27) Kuznetsov, A. E.; Boldyrev, A. I.; Zhai, H. J.; Li, X.; Wang, L. S. *J. Am. Chem. Soc.* **2002**, *124*, 11791.
(28) Li, X.; Zhang, H. F.; Wang, L. S.; Kuznetsov, A. E.; Cannon, N. A.; Boldyrev, A. I. *Angew. Chem., Int. Ed.* **2001**, *40*, 1867.
(29) Li, X.; Zhang, H. F.; Wang, L. S.; Geske, G. D.; Boldyrev, A. I. *Angew. Chem., Int. Ed.* **2000**, *39*, 3630.
(30) Geske, G. D.; Boldyrev, A. I.; Li, X.; Wang, L. S. *J. Chem. Phys.* **2000**, *113*, 5130.
(31) Cannon, N. A.; Boldyrev, A. I.; Li, X.; Wang, L. S. *J. Chem. Phys.* **2000**, *113*, 2671.
(32) Sierka, M.; Döbler, J.; Sauer, J.; Zhai, H. J.; Wang, L. S. *ChemPhysChem* **2009**, *10*, 2410.
(33) Meloni, G.; Ferguson, M. J.; Neumark, D. M. *Phys. Chem. Chem. Phys.* **2003**, *5*, 4073.
(34) Akin, F. A.; Jarrold, C. C. *J. Chem. Phys.* **2003**, *118*, 5841.
(35) Akin, F. A.; Jarrold, C. C. *J. Chem. Phys.* **2003**, *118*, 1773.
(36) Das, U.; Raghavachari, K.; Jarrold, C. C. *J. Chem. Phys.* **2005**, *122*, 014313.
(37) Santambrogio, G.; Janssens, E.; Li, S. H.; Siebert, T.; Meijer, G.; Asmis, K. R.; Döbler, J.; Sierka, M.; Sauer, J. *J. Am. Chem. Soc.* **2008**, *130*, 15143.
(38) Sierka, M.; Döbler, J.; Sauer, J.; Santambrogio, G.; Brummer, M.; Wöste, L.; Janssens, E.; Meijer, G.; Asmis, K. R. *Angew. Chem., Int. Ed.* **2007**, *46*, 3372.
(39) Feyel, S.; Döbler, J.; Höckendorf, R.; Beyer, M. K.; Sauer, J.; Schwarz, H. *Angew. Chem., Int. Ed.* **2008**, *47*, 1946.
(40) Schröder, D.; Fiedler, A.; Hrušák, J.; Schwarz, H. *J. Am. Chem. Soc.* **1992**, *114*, 1215.
(41) Kretzschmar, I.; Fiedler, A.; Harvey, J. N.; Schröder, D.; Schwarz, H. *J. Phys. Chem. A* **1997**, *101*, 6252.
(42) Ryan, M. F.; Fiedler, A.; Schröder, D.; Schwarz, H. *J. Am. Chem. Soc.* **1995**, *117*, 2033.
(43) Schröder, D.; Schwarz, H. *Angew. Chem., Int. Ed.* **1990**, *29*, 1433.
(44) Ryan, M. F.; Fiedler, A.; Schröder, D.; Schwarz, H. *Organometallics* **1994**, *13*, 4072.
(45) Dietl, N.; van der Linde, C.; Schlangen, M.; Beyer, M. K.; Schwarz, H. *Angew. Chem., Int. Ed.* **2011**, *50*, 4966.
(46) Harvey, J. N.; Diefenbach, M.; Schröder, D.; Schwarz, H. *Int. J. Mass Spectrom.* **1999**, *182*, 85.

(47) Kretzschmar, I.; Schröder, D.; Schwarz, H. *Int. J. Mass Spectrom. Ion Processes* **1997**, *167*−*168*, 103.
(48) Xu, X.; Faglioni, F.; Goddard, W. A. *J. Phys. Chem. A* **2002**, *106*, 7171.
(49) Irikura, K. K.; Beauchamp, J. L. *J. Am. Chem. Soc.* **1989**, *111*, 75.
(50) Feyel, S.; Döbler, J.; Schröder, D.; Sauer, J.; Schwarz, H. *Angew. Chem., Int. Ed.* **2006**, *45*, 4681.
(51) Schröder, D.; Roithová, J. *Angew. Chem., Int. Ed.* **2006**, *45*, 5705.
(52) Bozovic, A.; Bohme, D. K. *Phys. Chem. Chem. Phys.* **2009**, *11*, 5940.
(53) Chen, K.; Wang, Z. C.; Schlangen, M.; Wu, Y. D.; Zhang, X.; Schwarz, H. *Chem. Eur. J.* **2011**, *17*, 9619.
(54) Zhang, X.; Schwarz, H. *ChemCatChem* **2010**, *2*, 1391.
(55) de Petris, G.; Cartoni, A.; Troiani, A.; Barone, V.; Cimino, P.; Angelini, G.; Ursini, O. *Chem. Eur. J.* **2010**, *16*, 6234.
(56) de Petris, G.; Troiani, A.; Rosi, M.; Angelini, G.; Ursini, O. *Chem. Eur. J.* **2009**, *15*, 4248.
(57) Dietl, N.; Engeser, M.; Schwarz, H. *Chem. Eur. J.* **2010**, *16*, 4452.
(58) Dietl, N.; Engeser, M.; Schwarz, H. *Angew. Chem., Int. Ed.* **2009**, *48*, 4861.
(59) Dietl, N.; Engeser, M.; Schwarz, H. *Chem. Eur. J.* **2009**, *15*, 11100.
(60) Wang, Z. C.; Wu, X. N.; Zhao, Y. X.; Ma, J. B.; Ding, X. L.; He, S. G. *Chem. Phys. Lett.* **2010**, *489*, 25.
(61) Ma, J. B.; Wu, X. N.; Zhao, Y. X.; Ding, X. L.; He, S. G. *Phys. Chem. Chem. Phys.* **2010**, *12*, 12223.
(62) Dietl, N.; Höckendorf, R. F.; Schlangen, M.; Lerch, M.; Beyer, M. K.; Schwarz, H. *Angew. Chem., Int. Ed.* **2011**, *50*, 1430.
(63) Ding, X. L.; Zhao, Y. X.; Wu, X. N.; Wang, Z. C.; Ma, J. B.; He, S. G. *Chem. Eur. J.* **2010**, *16*, 11463.
(64) Ma, J. B.; Wu, X. N.; Zhao, Y. X.; Ding, X. L.; He, S. G. *J. Phys. Chem. A* **2010**, *114*, 10024.
(65) Eller, K.; Schwarz, H. *Int. J. Mass Spectrom. Ion Processes* **1989**, *93*, 243.
(66) Eller, K.; Zummack, W.; Schwarz, H. *J. Am. Chem. Soc.* **1990**, *112*, 621.
(67) Forbes, R. A.; Laukien, F. H.; Wronka, J. *Int. J. Mass Spectrom. Ion Processes* **1988**, *83*, 23.
(68) Schröder, D.; Schwarz, H.; Clemmer, D. E.; Chen, Y.; Armentrout, P. B.; Baranov, V. I.; Böhme, D. K. *Int. J. Mass Spectrom. Ion Processes* **1997**, *161*, 175.
(69) Sievers, H. L.; Grützmacher, H.-F.; Caravatti, P. *Int. J. Mass Spectrom. Ion Processes* **1996**, *157*−*158*, 233.
(70) Comisarow, M. B.; Grassi, V.; Parisod, G. *Chem. Phys. Lett.* **1978**, *57*, 413.
(71) Frisch, M. J., et al. *Gaussian 09, Revision A.02*; Gaussian, Inc., Wallingford, CT, 2009.
(72) Becke, A. D. *Phys. Rev. A* **1988**, *38*, 3098.
(73) Lee, C. T.; Yang, W. T.; Parr, R. G. *Phys. Rev. B* **1988**, *37*, 785.
(74) Becke, A. D. *J. Chem. Phys.* **1993**, *98*, 5648.
(75) Kohn, W.; Sham, L. J. *Phys. Rev.* **1965**, *140*, A1133.
(76) Schafer, A.; Huber, C.; Ahlrichs, R. *J. Chem. Phys.* **1994**, *100*, 5829.
(77) Feyel, S.; Schröder, D.; Rozanska, X.; Sauer, J.; Schwarz, H. *Angew. Chem., Int. Ed.* **2006**, *45*, 4677.
(78) Wang, Z. C.; Ding, X. L.; Ma, Y. P.; Cao, H.; Wu, X. N.; Zhao, Y. X.; He, S. G. *Chin. Sci. Bull.* **2009**, *54*, 2814.
(79) Zhao, Y. X.; Wu, X. N.; Wang, Z. C.; He, S. G.; Ding, X. L. *Chem. Commun.* **2010**, *46*, 1736.
(80) Zhao, Y. X.; Ding, X. L.; Ma, Y. P.; Wang, Z. C.; He, S. G. *Theor. Chem. Acc.* **2010**, *127*, 449.
(81) Ma, J. B.; Wu, X. N.; Zhao, Y. X.; He, S. G.; Ding, X. L. *Acta. Phys.-Chim. Sin.* **2010**, *26*, 1761.
(82) Zhai, H. J.; Döbler, J.; Sauer, J.; Wang, L. S. *J. Am. Chem. Soc.* **2007**, *129*, 13270.
(83) Wang, Z. C.; Xue, W.; Ma, Y. P.; Ding, X. L.; He, S. G.; Dong, F.; Heinbuch, S.; Rocca, J. J.; Bernstein, E. R. *J. Phys. Chem. A* **2008**, *112*, 5984.
(84) Dong, F.; Heinbuch, S.; Xie, Y.; Bernstein, E. R.; Rocca, J. J.; Wang, Z. C.; Ding, X. L.; He, S. G. *J. Am. Chem. Soc.* **2009**, *131*, 1057.
(85) Dong, F.; Heinbuch, S.; Xie, Y.; Rocca, J. J.; Bernstein, E. R.; Wang, Z. C.; Deng, K.; He, S. G. *J. Am. Chem. Soc.* **2008**, *130*, 1932.
(86) Schröder, D.; Roithová, J.; Alikhani, E.; Kwapien, K.; Sauer, J. *Chem. Eur. J.* **2010**, *16*, 4110.
(87) Wang, Z. C.; Wu, X. N.; Zhao, Y. X.; Ma, J. B.; Ding, X. L.; He, S. G. *Chem. Eur. J.* **2011**, *17*, 3449.
(88) Zhao, Y. X.; Wu, X. N.; Ma, J. B.; He, S. G.; Ding, X. L. *J. Phys. Chem. C* **2010**, *114*, 12271.
(89) Schlegel, H. B. *J. Comput. Chem.* **1982**, *3*, 214.
(90) Peng, C.; Ayala, P. Y.; Schlegel, H. B.; Frisch, M. J. *J. Comput. Chem.* **1996**, *17*, 49.
(91) Gonzalez, C.; Schlegel, H. B. *J. Chem. Phys.* **1989**, *90*, 2154.
(92) Gonzalez, C.; Schlegel, H. B. *J. Phys. Chem.* **1990**, *94*, 5523.
(93) Fukui, K. *J. Phys. Chem.* **1970**, *74*, 4161.
(94) Fukui, K. *Acc. Chem. Res.* **1981**, *14*, 363.
(95) Ruiz, E.; Cirera, J.; Alvarez, S. *Coord. Chem. Rev.* **2005**, *249*, 2649.
(96) Figgis, B. N.; Forsyth, J. B.; Reynolds, P. A. *Inorg. Chem.* **1987**, *26*, 101.
(97) Fiedler, A.; Kretzschmar, I.; Schröder, D.; Schwarz, H. *J. Am. Chem. Soc.* **1996**, *118*, 9941.
(98) Feyel, S.; Schröder, D.; Schwarz, H. *Eur. J. Inorg. Chem.* **2008**, *2008*, 4961.
(99) Jackson, P.; Harvey, J. N.; Schröder, D.; Schwarz, H. *Int. J. Mass Spectrom.* **2001**, *204*, 233.
(100) Bärsch, S.; Schröder, D.; Schwarz, H. *Chem. Eur. J.* **2000**, *6*, 1789.
(101) Asmis, K. R.; Meijer, G.; Brummer, M.; Kaposta, C.; Santambrogio, G.; Wöste, L.; Sauer, J. *J. Chem. Phys.* **2004**, *120*, 6461.
(102) Solans-Monfort, X.; Branchadell, V.; Sodupe, M.; Sierka, M.; Sauer, J. *J. Chem. Phys.* **2004**, *121*, 6034.
(103) Kwapien, K.; Sierka, M.; Döbler, J.; Sauer, J.; Haertelt, M.; Fielicke, A.; Meijer, G. *Angew. Chem., Int. Ed.* **2011**, *50*, 1716.
(104) To, J.; Sokol, A. A.; French, S. A.; Kaltsoyannis, N.; Catlow, C. R. A. *J. Chem. Phys.* **2005**, *122*, 144704.
(105) Pacchioni, G.; Frigoli, F.; Ricci, D.; Weil, J. A. *Phys. Rev. B: Condens. Matter Mater. Phys.* **2001**, *63*, 054102.
(106) Kwapien, K.; Sierka, M.; Döbler, J.; Sauer, J. *ChemCatChem* **2010**, *2*, 819.
(107) Noodleman, L. *J. Chem. Phys.* **1981**, *74*, 5737.
(108) Noodleman, L.; Case, D. A.; Aizman, A. *J. Am. Chem. Soc.* **1988**, *110*, 1001.
(109) Soda, T.; Kitagawa, Y.; Onishi, T.; Takano, Y.; Shigeta, Y.; Nagao, H.; Yoshioka, Y.; Yamaguchi, K. *Chem. Phys. Lett.* **2000**, *319*, 223.
(110) Wang, Z. C.; Weiske, T.; Schlangen, M.; Schwarz, H. Unpublished results.
(111) Jahavery, G.; Becker, H.; Petrie, S.; Cheng, P. C.; Schwarz, H.; Scott, L. T.; Bohme, D. K. *Org. Mass Spectrom.* **1993**, *28*, 1005.